Final Report

Droplet Interaction with Hot Surfaces

Prepared by

Yudaya Sivathanu
En'Urga Inc.
1291 Cumberland Avenue
West Lafayette, IN 47906

and

Harsh P. Oke, Chunming Fu, Tony Wang and Paul E. Sojka
Maurice J. Zucrow Laboratories
School of Mechanical Engineering
Purdue University
West Lafayette, IN 47907-1003

Prepared for

Dr. Richard Gann
NGP Technical Program Manager
Chief, Fire Sciences Division
Building and Fire Research Laboratory, Bldg. 224, Rm. B250
National Institute of Standards and Technology
Gaithersburg, MD 20899

Contract Number: DASW01-98-C-0029

March, 2000

En'Urga Inc.

ANALYSIS OF COMBUSTION SYSTEMS

Droplet Interaction with Hot Surfaces

Yudaya Sivathanu
En'Urga Inc.
1291 Cumberland Avenue
West Lafayette, IN 47906

and

Harsh P. Oke, Chunming Fu, Tony Wang and Paul E. Sojka
Maurice J. Zucrow Laboratories
School of Mechanical Engineering
Purdue University
West Lafayette, IN 47907-1003

Contract Number: DASW01-98-C-0029

Yudaya Sivathanu

March, 2000

Acknowledgement

The work in this report was supported by the SERDP Next Generation Fire Suppression Technology Program under contract No. DASW01-98-C-0029. Dr. Richard Gann served at the NGP Technical Program Manager for the contract. The authors are solely responsible for the entire contents of this report.

EXECUTIVE SUMMARY

The objective of the project was to study the interaction between droplets and burning surfaces so as to engineer better fire suppressants. The project consisted of two parts. The first part determined the effect of water mist on the suppression of flame spread over a solid fuel. The second part examined the role of buoyancy and evaporation on the droplet size and velocity distributions as they approach a hot surface.

The effect of water mist on the reduction in flame spread velocity was obtained by experiments conducted in a wind tunnel. Flame spread velocities with and without the water mist were obtained for a solid fuel, polymethyl methacrylate (PMMA) using Focal Plane Array Imaging. PMMA sheets of different thickness were burned in an opposed flow configuration, with varying wind velocities. A spray nozzle, suspended over the PMMA sheets, was used to vary the water loading at the flame front.

In the presence of water mist, the flame spread rate is a strong function of the water loading on the fuel surface. As the loading increases, the flame spread rate decreases. The effect is more pronounced at low values of opposing wind speeds. The effect of mean drop size of the spray on flame spread rate was small for the range of droplet sizes used in the experiments. An empirical correlation of the water loading required to retard the spread of unwanted fires and to extinguish them was developed. The results of the study will be directly applicable to designing fire suppressant devices so that the minimum mass of suppressant is applied directly to the fire.

The total water loading at the fire location depends on the trajectory of droplets through the fire. Two physical effects that change the trajectory and size of droplets are evaporation and buoyancy induced local air velocity. A non-evaporating spray (Dow Thermal Fluid 510) was used to assess the effects of buoyancy induced air velocity on droplet size and trajectory. An evaporating spray (water) was used to study the combined effects of buoyancy induced flow as well as evaporation on the droplet trajectories. The results show that coalescence is the dominant mechanism by which droplets change size during their flight to the hot surface.

The data was used to evaluate two models for droplet coalescence and evaporation. The results showed that these models have to be improved significantly before they can be directly used in fire suppression studies.

Table of Contents

Acknowledgement 1

Executive Summary 2

1. Introduction 4
- 1.1 Project Objective 4
- 1.2 Background 4
- 1.3 Technical Approach 5

2. Flame Spread Studies 6
- 2.1 Experimental Methods 6
- 2.2 Results and Discussion 9

3. Droplet Interactions with a Hot Surface 16
- 3.1 Experimental Methods 16
- 3.2 Numerical Methods 21
- 3.3 Results and Discussion 23
- 3.3 Preliminary Model Results 27

4. Summary Conclusion 27
- 4.1 Important Findings 27
- 4.2 Significant Hardware Development 28
- 4.3 Recommendations for Future Research 28
- 4.4 List of Publications 28

4. Implications for Further Research 28

References 29

DROPLET INTERACTION WITH HOT SURFACES

1. Introduction

1.1 Project Objective

To obtain data and an understanding of the interaction of droplets with burning surfaces required to engineer improved heterogeneous agent dispersion systems with enhanced fire-extinction capability.

1.2 Background

Currently, most fire suppression devices, particularly for aerospace and military applications, utilize Halon 1301 as the suppressant. Halon 1301 has been discontinued due to environmental concerns, and a search for alternate suppressants is underway. This has lead to a renewed interest in the fundamental fire suppression mechanisms.

There have been numerous studies on flame spread velocities in opposed and counter flow configurations (De Ris, 1969; Lastrina et al., 1971, Fernandez-Pello *et al.*, 1978; Fernandez-Pello *et al.*, 1981, Apte *et al.*, 1991; Loh and Fernandez-Pello, 1984; Perzak and Lazzara, 1992) during the last three decades. These studies have shown that the flame spread velocity depends on the fuel thickness, flow configuration, oxygen concentration, and the size of the wind tunnel. Therefore, for flame suppression studies, it is best to obtain data with and without the suppressant in the same facility.

Interactions of water mists with fires have been studied for almost four decades (Braidech et al., 1955; Rasbash et al., 1960; Lugar, 1979; Mawhinney *et al.*, 1994; Coppalle *et al.*, 1993). The major pathways to extinction of fires involve heat extraction, oxygen reduction, concentration changes in vapor/air mixtures and kinetic effects at the molecular level. Braidech et al. (1955) have concluded correctly that, in most cases, the efficacy of water mist is predominantly due to the oxygen displacement effect of the water evaporating, rather than to thermal cooling. However, there are no detailed models describing the size reduction and evaporation of droplets in flames, or their effect on surface reaction kinetics. Indeed, even models that predict what size droplets will reach the surface are not available.

Studies describing spray-target interactions have primarily focused on application of paints/coatings to surfaces (Kwok, 1991, Hicks and Senser, 1995). These studies have shown that high gas phase strain rates where the spray impinges on the target dramatically affect turbulent transport of small (diameter less than 25 μm) droplets, and hence the deposition of the said droplets on the intended surface. In addition, the deposited drop size distribution can be significantly different from that of the (initial) spray. Finally, drop transport is dependent on initial drop momentum, aerodynamic drag, and the gravitational force, with aerodynamic drag being dominant.

Many studies have been performed that quantify the vaporization process of both single and multiple droplet arrays impacting on hot surfaces (DiMarzo and Evans, 1986; DiMarzo et al., 1989). These studies have identified the need for spatially and temporally resolved data describing the droplet trajectory as it approaches a hot surface (including buoyancy effects) as well as the temperature distribution of the surface material.

The present study seeks further understanding of the interaction of droplets with fires in two areas. First, this study experimentally determines the key water mist properties, such as surface loading and droplet diameter, that affect flame spread rate. It is hoped that the data will lead to improved fire extinguishing agents and suppression methods. Secon, this study seeks to numerically and experimentally determine the droplet size and velocity history as it approaches a hot surface or fire.

Direct Simulation Monte Carlo is widely used to solve for the heat transfer in a wide variety of problems (Howell, 1968; Haji-Sheik, 1988) due to its simplicity and accuracy. There are many methods to improve the accuracy of Monte-Carlo simulations which include importance sampling (Kahn and Marshall, 1953), weighing and biasing (Lanore, 1971), and the discrete probability function method (Sivathanu and Gore, 1993). Therefore, the simulation of the problem utilizing Monte-Carlo methods is straightforward, once the important rates that govern the physical processes are understood.

The different components that describe both the droplet trajectory and the temperature distribution over the surface as a function of time are studied in detail in this project by separating the various physical processes and integrating them to obtain an experimentally validated model that can be used in Monte-Carlo simulations.

1.3 Technical Approach

- Conduct experiments with non-evaporating and evaporating particles of controlled density injected at controlled velocities towards a variably heated surface.
- Obtain the variation in particle velocity as a function of the impressed buoyancy forces, thereby determining the effects of flame buoyancy on the likelihood of a particle reaching a burning surface.
- Determine the effect of evaporation on these results.
- Conduct experiments with mono-disperse and poly-disperse droplets injected over the flames from PMMA or over heated polyurethane foam, using droplet loading, delay time after ignition, and location of the spray from the leading edge as parameters.
- Obtain reduction in flame spread so as to obtain empirical correlation between spray characteristics and flame spread.
- Use a Two Color Planar Pyrometer to measure surface temperature changes as a function of aerosol impingement.
- Conduct Monte-Carlo simulations of the mist/surface interactions to develop fuller understanding of the dominant processes and identify the key aerosol properties that impact efficient suppression of the fire.

2. Flame Spread Studies

The primary objective of this work is to determine the effect of water mist on flame spread rate and develop an empirical correlation that can be used to design fore suppression systems. The variation of flame spread rate with the surface loading of water and the diameter of the droplets is the focus of this part of the study.

2.1 Experimental Methods

The flame spread experiments were carried out in a wind tunnel, whose photograph is shown in Fig. 1. The wind tunnel is of a rectangular cross-section 45 cm high and 76 cm

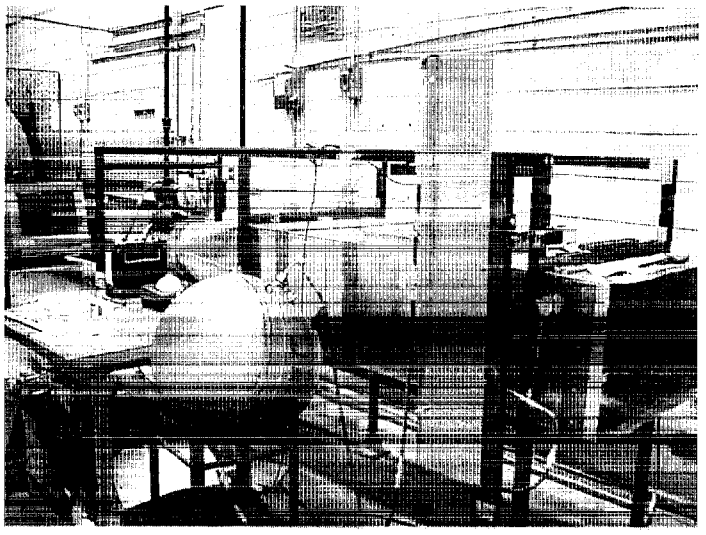

Figure 1. Wind tunnel used for fire spread studies.

Wide and 1.75 m long. The roof has three rectangular slots 7.6 cm wide x 28 cm long for observation of the flame by means of a video camera. The slots are covered with 12.5 mm thick glass windows during experiments. The velocity inside the tunnel is control by a DC motor driven exhaust fan.

Honeycomb flow straighteners of polycarbonate placed at the mouth of the duct, are used to remove large scale turbulent eddies and create uniform flow conditions in the test section. Each flow straightener has a diameter of 6.4 mm and is 25 cm in length. This L/D ratio, yields a maximum Reynolds number of 64 and is sufficient to establish a fully developed laminar flow in the straighteners (Fox and McDonald, 1994). A 1.6 mm thick ceramic paper was applie d to the interior of the tunnel to reduce heat transfer to the walls.

PMMA supports surface combustion, and the flame spread rate over it is steady and well characterized. The properties of PMMA, such as density, specific heat at constant pressure, and heat of combustion, are consistent and well known. Therefore, PMMA was used in the present study.

30 cm x 20 cm PMMA sheets having thickness of 3.2 and 6.4 mm were used for the present study. The PMMA sheets were ignited with a small methanol trough before placing them into the wind tunnel. The experiments were carried out at four opposing wind speeds of 0.69, 0.84, 1.21, and 1.53 m/s. Three flow rates, ranging from 9.5 to 15.5 cc/min, and three inlet pressures (880, 1375, and 2115 kPa) were used to vary the mass loading and the droplet size of the water spray used for suppression.

Initially, the fire suppression experiments were carried out with one surface in contact with an insulating ceramic material. This is the conventional method, called here 'with backing' mode or one-sided combustion mode. When fire suppression experiments were begun, it was realized that the ceramic backing was quick to absorb water and was instrumental in extinguishing the flame almost as soon as the water spray was turned on. Therefore, the present studies were carried out with the PMMA sample supported along its sides with air flowing above and below the specimen. A photograph of the flame suppression experiment with the water mist applied is shown in Figure. 2.

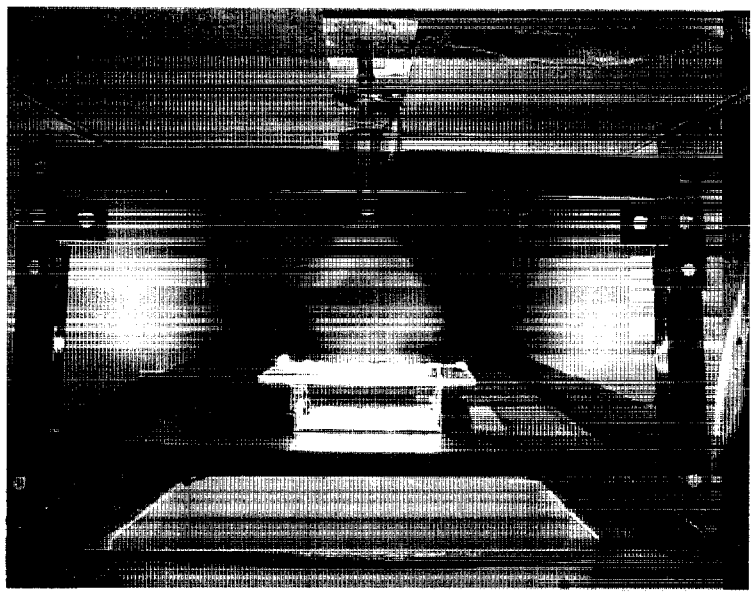

Figure 2. Flame spread experiment with water mist.

Calculations showed that the Blasius boundary layer thickness over the surface of the aluminum platform has a maximum value of about 1.4 cm. By keeping a 6 cm gap between the bottom surface of the PMMA specimens and the support platform, it was ensured that free stream conditions existed on both the top and bottom and that the flame spread was unaffected by the boundary layer on the support platform.

A hollow cone spray was generated using a pressure atomizer which delivers good atomization quality over a large range of flow rates at the same inlet pressure. The nozzle is mounted on a bracket at a distance of about 60 cm upstream of the sample and at a

height of about 17.5 cm above the surface of the PMMA. The droplets are carried downstream and onto the flame by the airflow present in the wind tunnel.

To obtain local surface loading of the water spray, pieces of absorbent tissue paper were taped onto the surface of a PMMA sample in a 4 x 4 grid. The spray was established at a given test condition and the difference in weight of the tissues was determined after a suitable interval of time. A Phase Doppler Particle Analyzer was used to obtain the drop size and drop mean velocity data. The PDPA was operated in forward scatter mode ($\theta=30^{\circ}$). The probe volume was 14 cm downstream of the nozzle exit.

A black-and-white 8-bit CCD camera was used to track the motion of the flame. The camera is mounted on a bracket above the observation window and looks down perpendicularly onto the burning samples. It was observed that the edges of the PMMA samples burn faster than the center. In order to avoid erroneous estimates of flame spread rate on account of edge effects, the camera focused on the central 23 cm of the flame.

During a typical experiment, the flame spread images were obtained 8 seconds apart. The location of the flame was defined to be the pixel of maximum intensity value. The difference in location of the flame in a particular row of pixels between two frames (that are separated by a known time interval) yielded the flame spread rate for that row. To reduce the discretization errors, the flame spread was calculated from images separated by 160 seconds. The mean velocity of the flame calculated for all the rows was designated to be the velocity of the flame at that time.

The reduction in flame temperature due to droplet loading was obtained using a two color planar pyrometer (TCPP). A schematic diagram of the two color planar pyrometer is shown in Fig. 3. The TCPP has an imaging lens that is used to collect broad band

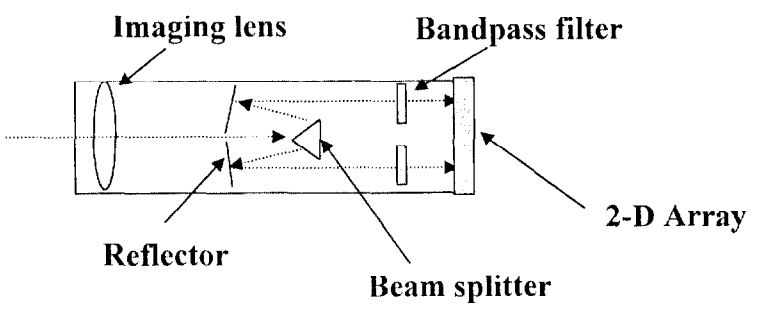

Figure 3. Schematic of the two color planar pyrometer.

radiation from the fire. The radiation is split into two and spectrally differentiated using band pass filters. An array imaging camera is used to obtain the spectral image of the flame at two wavelengths. For the present study, the band pass filters were centered at approximately 900 and 1000 nm, and each had a band width of 80 nm. The TCPP was calibrated using a standard laboratory black body source.

2.2 Results and Discussion

The first issue addressed is the measurement uncertainty. If x is the position of the flame and t is the time interval between measurements, the velocity is given by v=x/t. The uncertainties in the measurement of flame position (w_x) and time (w_t) can be used (Kline and McClintock, 1953) to estimate the uncertainty in the flame spread rate (w_v) as:

$$w_v = \left[\left(\frac{\partial v}{\partial t} w_v \right)^2 + \left(\frac{\partial v}{\partial x} w_x \right)^2 \right]^{1/2} \tag{1}$$

For the imaging system, the uncertainty in position is ± 1 pixel, and that in time (provided by the camera timer) is 1 microsecond. Therefore, for a typical flame event lasting 160 s, with the flame moving about 12 pixels, the uncertainty in velocity is:

$$\frac{w_v}{v} = \frac{w_x}{x} = 8.3\% \tag{2}$$

Typical flame velocity data obtained using the imaging system is shown in Fig. 4.

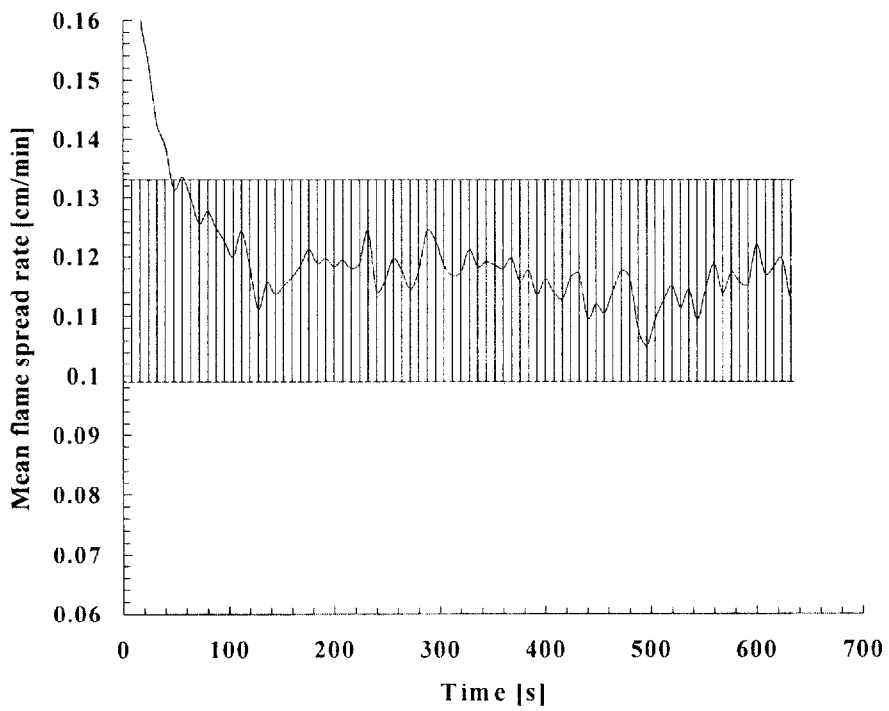

Figure 4. Typical flame spread time trace obtained using Focal Plane Array Imaging.

As soon as the flame is lit, the imaging system starts obtaining data at a rate of 1 image every eight seconds. During the first few minutes, the flame spread rate rapidly decreases until a steady state is reached. At steady state, the flame spread velocity changes

approximately ± 10% due to the small scale fluctuations in the flame front and the uncertainty of the measurement.

The flame spread rate as a function of opposing wind speed is shown in Fig. 5. The vertical bars represent one standard deviation in the statistical variation of the data on

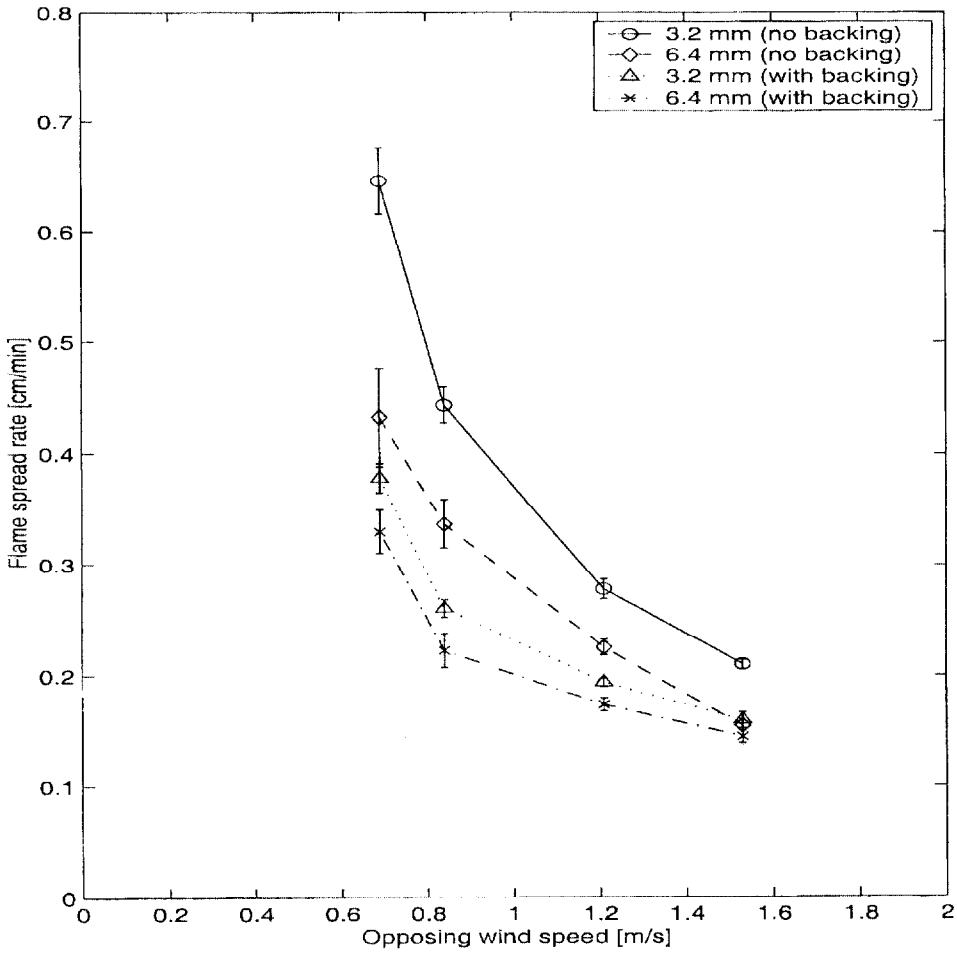

Figure 5. Flame spread rates without the water mist.

each side of the mean (approximately 60 points per run). The experimental uncertainty is less than 10% of the mean.

The expected result is seen that the flame spread rate without backing is higher than that with backing for the same sample thickness since burning is allowed to take place on both sides in the 'without backing' mode. Also in 'with backing' mode, some amount of heat loss occurs to the supporting aluminum plate since the ceramic paper (on which the PMMA is burned) is not a perfect insulator.

Another observation is that the flame spread rate decreases as the opposing wind speed increases. This can be explained by realizing that the forward heat transfer by gas-

phase conduction from the flame to the unburned fuel decreases. Convective heat transfer from the unburned fuel surface also increases. This result is therefore expected. It is also found that the flame spread rate is higher for the thinner fuel than the thicker fuel. Since the heat transfer required to raise the temperature of the unburned fuel to its vaporization temperature is less for a thin fuel, this finding is also expected. These three results are consistent with the observations of previous investigators.

The flame spread rate results found in this work are approximately 20% greater than the findings of Fernandez-Pello *et al.* (1981) for the 6.4 mm thickness PMMA at 0.7 m/s opposed flow velocity. At flow velocities of 0.85 and 1.2 m/s, the results in the present work are lower than the findings of Fernandez-Pello *et al.* (1981) by about 9 and 6%, respectively. The results are all within the limits of experimental uncertainty.

Any differences that exist beyond experimental uncertainty can be explained as follows. At the lower opposed wind speeds the flame stand-off height is more than at the higher opposed wind speeds. As the width of the sample in the present work (30 cm) is much greater than that in the work of Fernandez-Pello *et al.* (1981), there is greater radiation heating of the unburned fuel surface by the flame. Hence the measured flame spread rate is greater.

At the higher opposing wind speeds the flame stand-off height is much less. At these high wind speeds,radiation from the flame is much lower (on account of a small view factor). It is believed that it is the size of the experimental facility that is responsible for differences in the measured flame spread velocities between this study and the work of Fernandez-Pello *et al.* (1981). In particular, the wind tunnel duct used by Fernandez-Pello *et al.* (1981) is 5 cm x 4 cm in cross-section and 1 m long while the duct used in the present work has a cross-section of 45 cm x 76 cm and is 1.75 m long. The greater re-radiation from the walls of the duct in the work of Fernandez-Pello *et al.* (1981) is believed to be the reason for the difference in the findings.

Another reason for the differences between the current measurements and those of Fernandez-Pello et al. could be different diagnostic and analytical techniques used to determine the flame spread rate. The progress of the flame in the experiments of Fernandez-Pello *et al.* was measured visually as it passed over previously ruled marks on the PMMA surface, whereas in the present work a CCD camera tracked the flame motion. The data analysis method used by Fernandez-Pello *et al.* is not known, but in the present work the estimate of flame spread rate is over a rather large length of time (160 seconds) rather than being 'instantaneous'.

The flame spread rate as a function of surface loading for the 3.2 mm thickness sample is shown in Figure 6. Similar results for the 6.4 mm thick PMMA are shown in Fig. 7. The systematic decrease in flame spread rate with increasing surface loading on the PMMA can be clearly seen in all cases.

The effect of surface loading appears to be greatest in the case of low opposing wind speeds, viz. 0.69 and 0.84 m/s. The reason may be that the flame spread rate is low

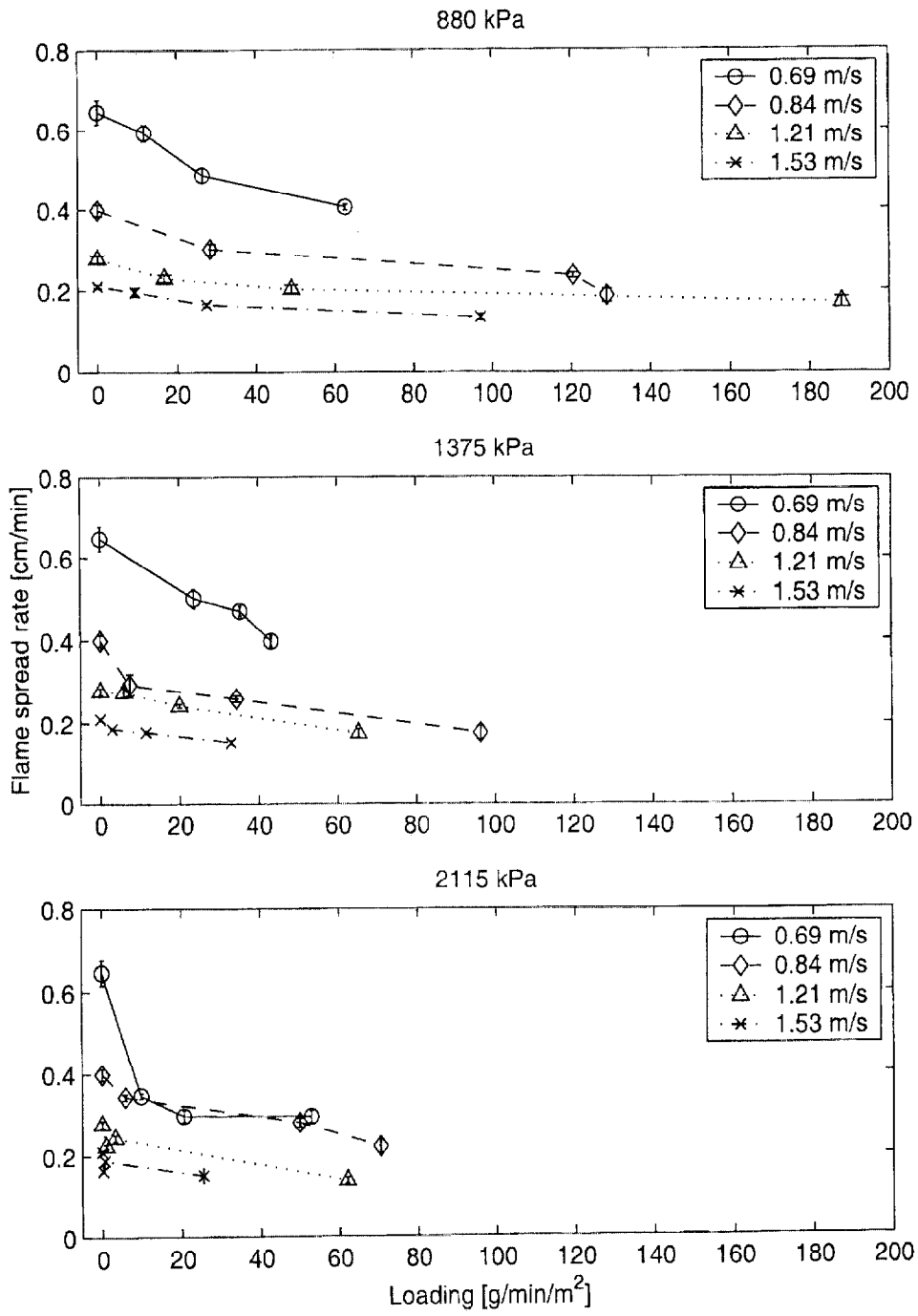

Figure 6. Flame spread rate as a function of surface loading for 3.2 mm thick PMMA.

to begin with at the higher opposing wind speeds and with increasing loading there is a practical limit to the flame spread rate that can exist and still be measurable. It is conjectured that a threshold value of flame spread rate exists, between 0.15 and 0.20 cm/min, below which the flame will be rapidly extinguished.

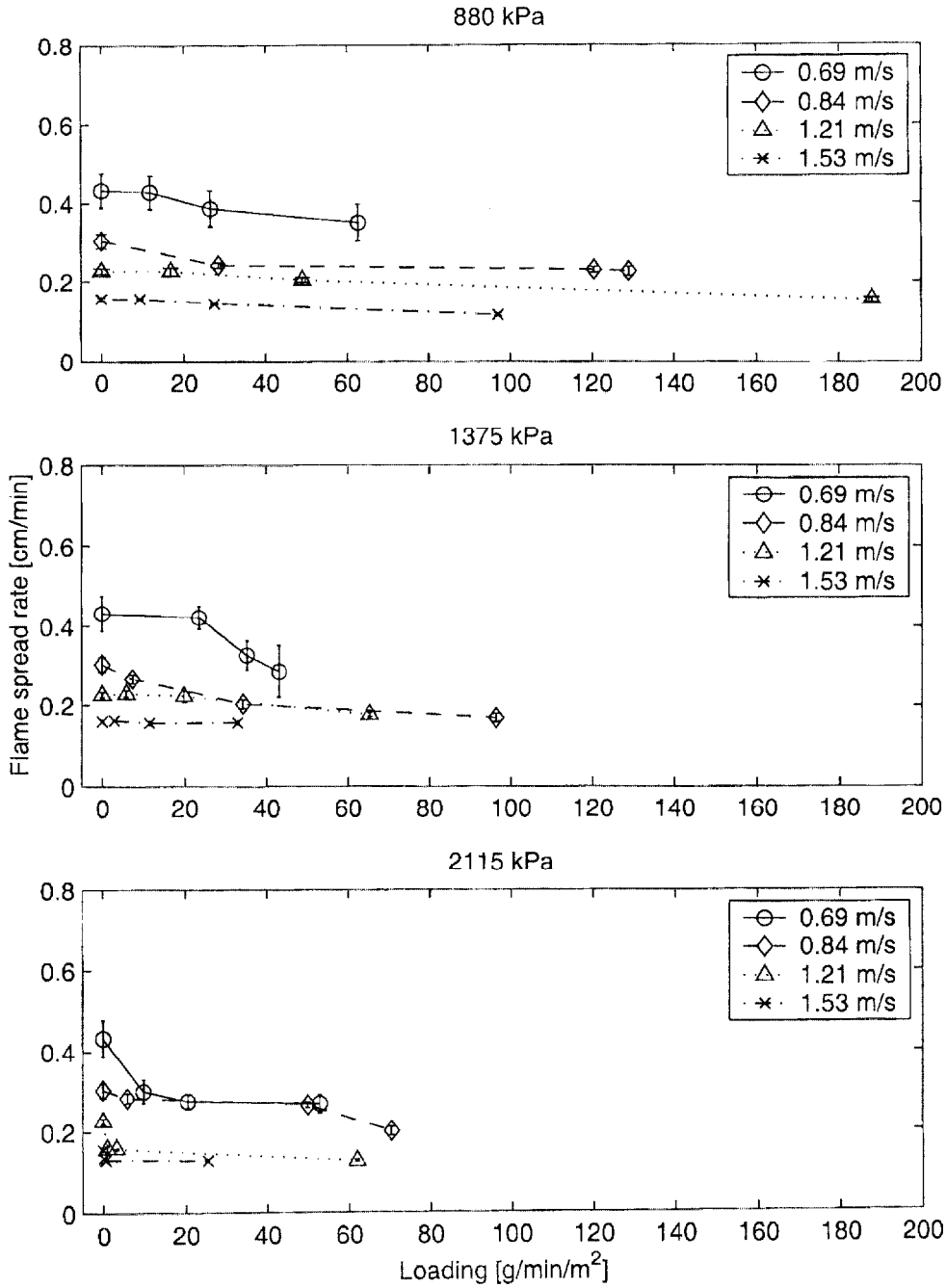

Figure 7. Flame spread rate as a function of surface loading for 6.4 mm thick PMMA.

The role of surface loading on the flame spread rate can be explained in terms of heat transfer effects. On account of surface cooling there is a reduction in pyrolysis of the fuel ahead of the flame front. As the rate of fuel vapor production decreases, less heat is liberated in the exothermic chemical reaction between the fuel vapor and oxygen. This

results in a net decrease in heat transfer to the unburned PMMA ahead of the flame. As a result, the flame spread rate drops.

In order to determine the effect of spray operating parameters on the droplet size, namely the atomizer inlet pressure and flow rate, measurements of drop size and velocity were performed using a Phase/Doppler Particle Analyzer. Drop size and velocity data are presented in Figure 8.

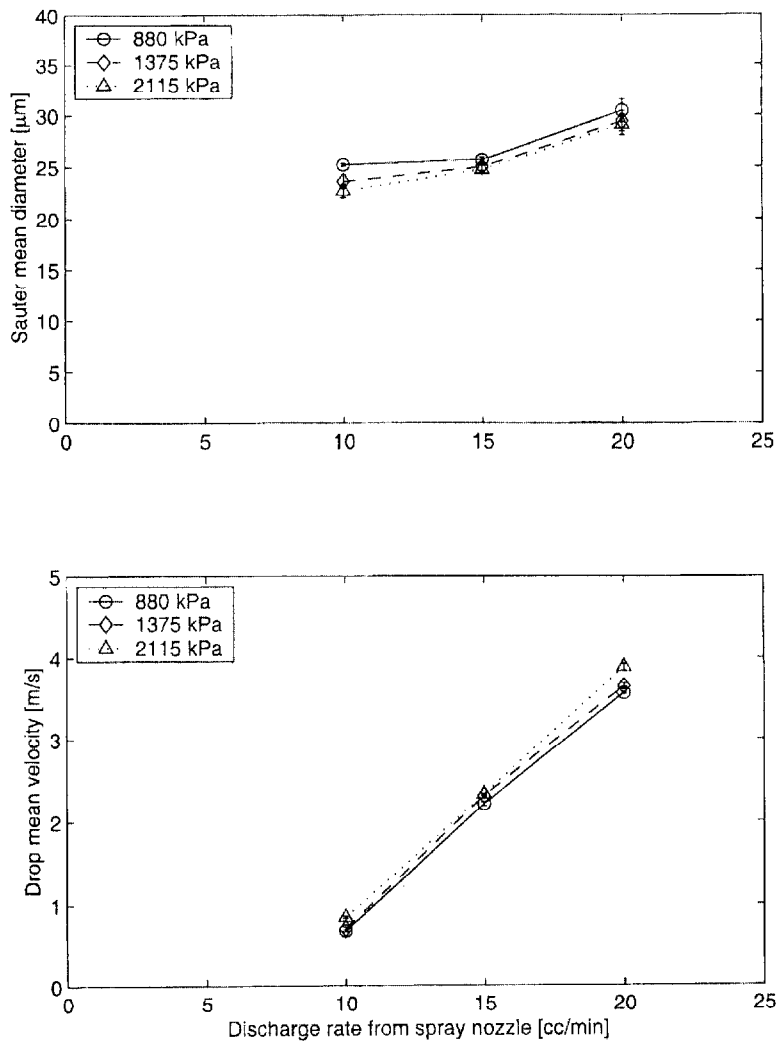

Figure 8. Mean drop size and velocity as a function of spray nozzle discharge rate.

From Figure 8 it is seen that both the drop size and the mean velocity increase as the mass flow rate through the nozzle increases for a constant inlet pressure. At the same flow rate through the nozzle, the drop size is smaller and the mean velocity greater at the higher pressure. The difference in the mean drop diameter at 10 cc/min flow rate at the three different pressures is approximately 2.5 μm; at 15 cc/min flow rate it is approximately 1 μm. By the d^2-law of droplet evaporation the ratio of evaporation times of drops 27.5 and

25 μm in diameter is 1.2. Therefore, a notable impact due to evaporative cooling in the flame vicinity cannot be expected. Consequently, the drop size variation should not be a significant factor in flame spread rate variations for the conditions considered here.

The drop mean velocity measurements provide an explanation as to why the flame spread rate increases with increasing nozzle discharge rate at low opposing wind speeds. The reason is that the drop mean velocity increases as the flow rate increases. This reduces drift due to the cross-wind and leads to deposition of the spray in the collection pan (placed below the spray nozzle) upstream of the target. The surface loading on the PMMA is thus reduced and, consequently, the flame spread rate increases.

The data obtained from all tests were used to develop an empirical correlation. The normalized flame spread rates for all conditions are shown in Fig. 9. Three different

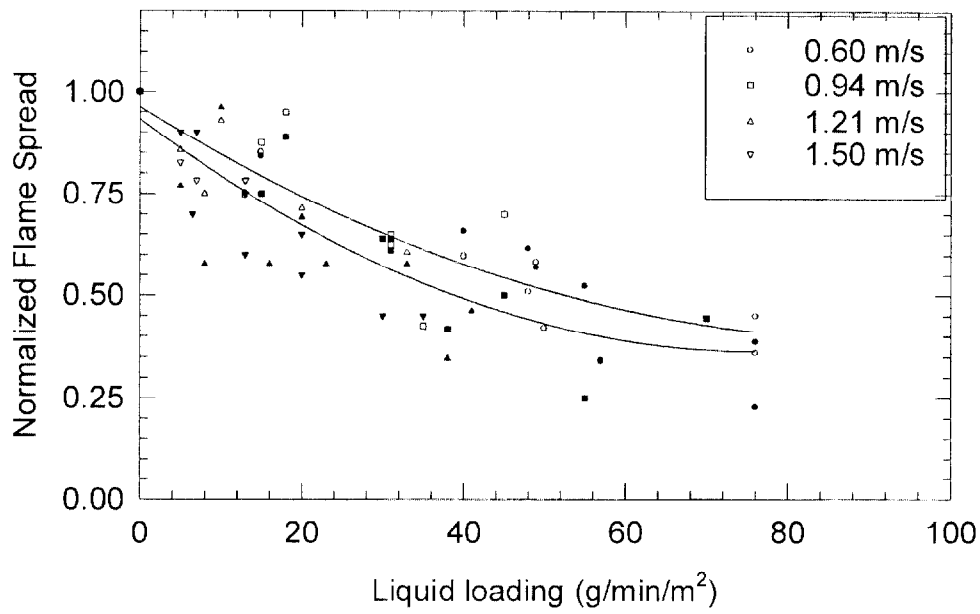

Figure 9. Variation in normalized flame spread with liquid loading.

injection pressures (corresponding to different droplet diameters), two different PMMA thickness, and four different opposed flow velocities were used in developing the empirical correlation.

Data represented by open symbols shown in Fig. 8 were obtained with 3.2 mm thick PMMA, and those represented by closed symbols were obtained with 6.4 mm thick PMMA sheets. The regression analysis for the normalized flame spread in the thinner samples provides an approximately 85% correlation with liquid mass loading. For the thicker samples, the correlation of the normalized flame spread with the liquid mass loading is approximately 75%. The correlation obtained for all twenty-four conditions show that the

normalized flame spread rate can be roughly expressed as a function of the local liquid mass loading alone Correlations for flame spread rates with zero liquid mass loadings are readily available in literature. Therefore, the current results can be used to estimate (within a factor of two) what the local liquid mass flux should be to achieve extinction. This information is useful, since it would provide a direct estimate of the optimal suppressant mass required to extinguish fires.

The effect on water loading on the decrease in the mean flame temperature is shown in Fig. 10. The mean temperature of the flame without any water loading varies

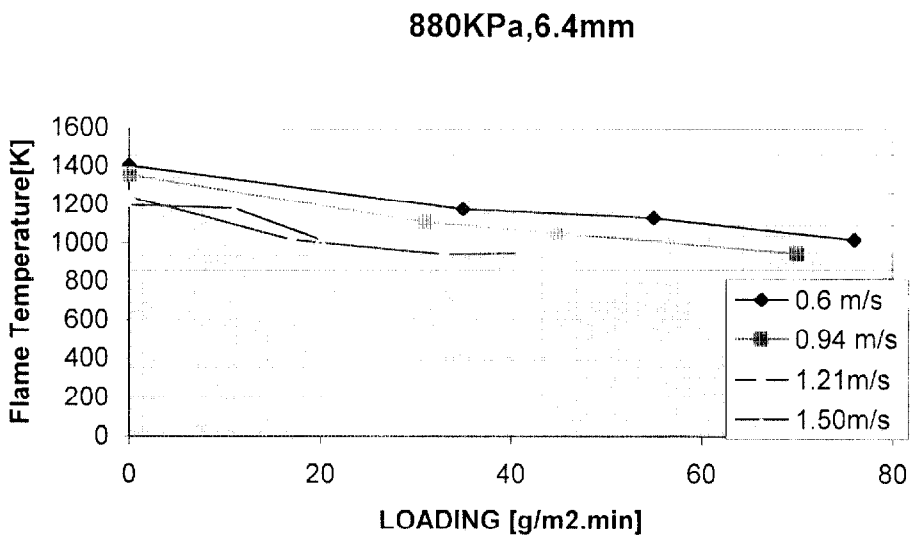

Figure 10. Mean flame temperature obtained using the TCPP.

Between 1200 and 1400 K depending on the opposing wind velocity. In general, when the opposing wind velocity is high, the flame temperature is lower due to effects of flame stretch. This temperature drops rapidly with increasing water loading and the flame is extinguished at approximately 1000 K.

3. Droplet Interaction with a Hot Surface

3.1 Experimental Methods

The second part of hardware development involved fabrication of a heated surface to obtain the simultaneous drop size and velocity distributions for a spray impinging on a hot target. The schematic of this experimental arrangement is shown in Fig. 11.

The experimental apparatus consisted of six main parts: the liquid supply system, the piezoelectric ceramic atomizer and its power supply system, the heater assembly and its power supply system, the temperature data acquisition system, the Phase Doppler Particle Sizer (PDPA) spray characterization system, and the spray imaging system.

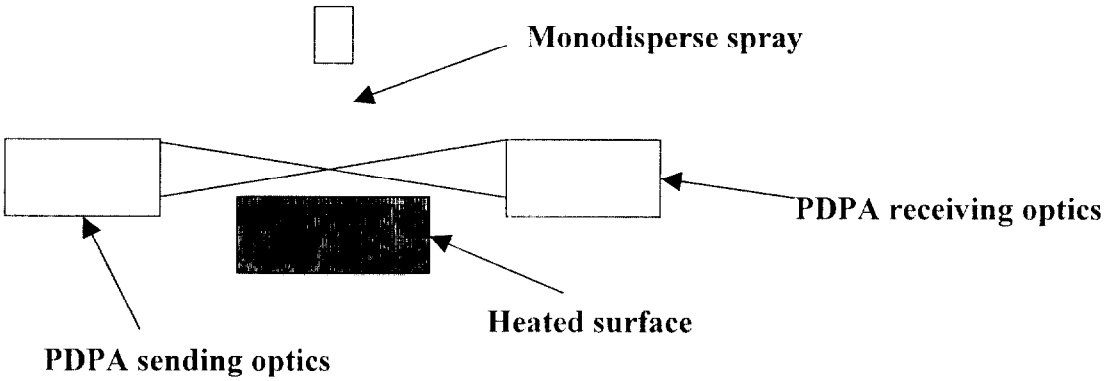

Figure 11. Experimental arrangement for the PDPA measurements.

Compressed shop air was reduced to an appropriate pressure by a regulator then introduced into a thick-walled plastic tank. Liquid flowed out of the tank, passed through a filter and a rotameter, before finally reaching the piezoelectric ceramic atomizer. The filter had a pore size of 10 μm. The mass flow rate ranged from 0.1 to1.0 g/s, and the inlet pressure ranged from 27.6 to 82.7 kPa. They were adjusted simultaneously using the rotameter. Distilled water was used for evaporation experiments. A non-evaporative liquid purchased from Dow Corning, Fluid 510, was used for the buoyancy experiments.

A piezoelectric atomizer, purchased from Universität Erlangen-Nürnberg in Germany was used to produce monodisperse droplets (Brenn et al., 1997) with flow rates up to 4 g/s. A schematic of the atomizer is shown in Fig. 12. A 2 MHz function generator (Model 19

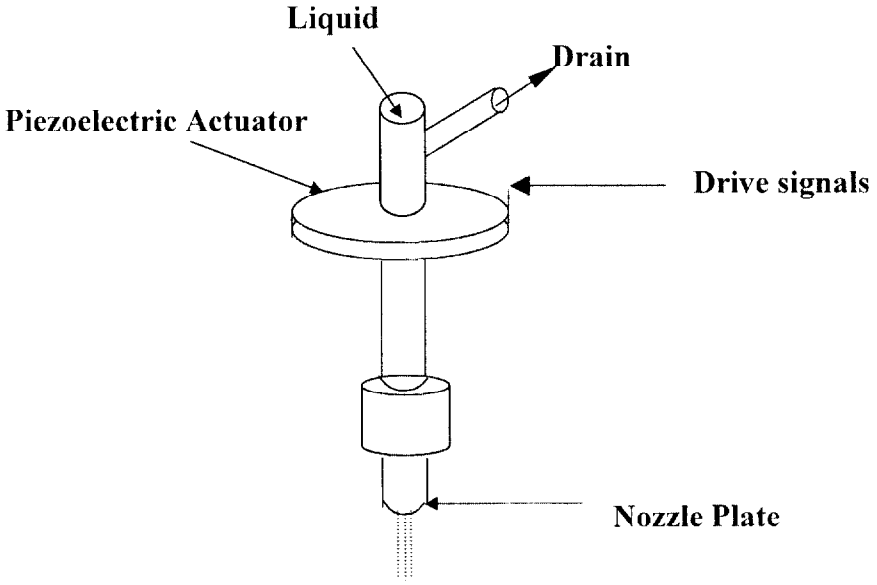

Figure 12. Configuration of the piezoelectric atomizer.

from Wavetek) was used with an amplifier to supply square wave signals (approx 30 V peak to peak) to the atomizer. Output frequencies ranged from 3 kHz to 2 MHz.

Three round stainless steel plates with orifices of different diameters made by laser drilling were used as nozzles in the atomizer. The plates are 50 μm thick, and are supported by a 1mm thick stainless plate with a 1mm hole in the center. The orifice diameters were 100, 50, and 20 μm. The atomizer was placed above the center of the heater in a fixture that allowed 360 degree rotation. In addition, the atomizer was capable of being moved in both the vertical and horizontal direction.

A heat source is necessary to provide a surface temperature as uniform as possible. A modified design of a hot plate designed by Dingel (1995) was used in the experiments. A schematic of the heater assembly is shown in Fig. 13. The main components are an

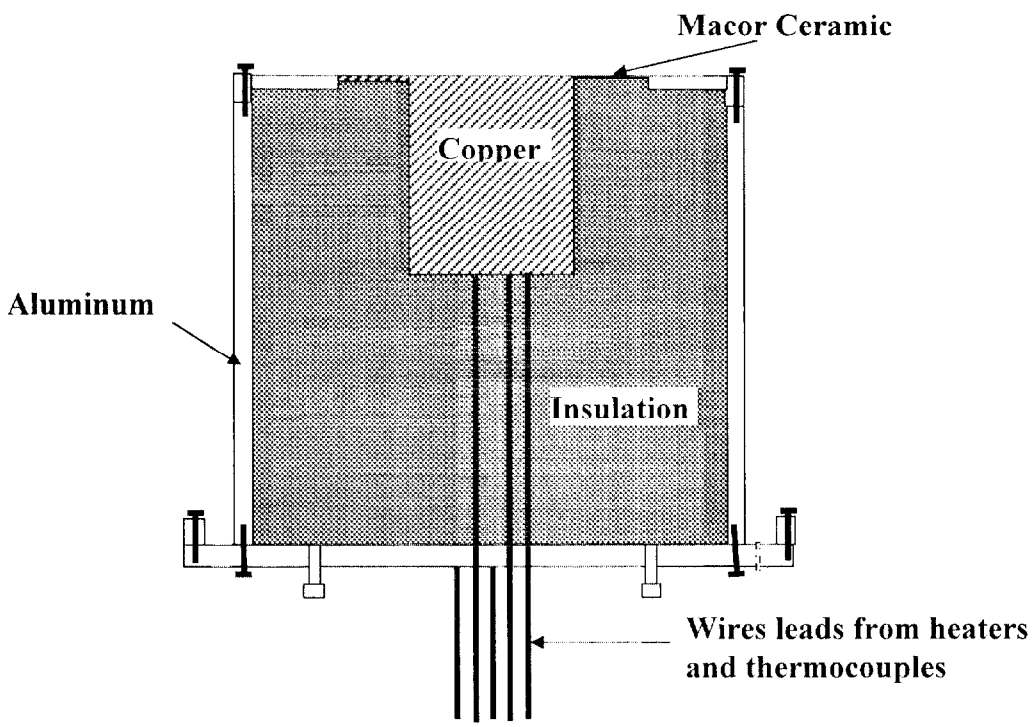

Figure 13. Schematic diagram of the heater assembly.

exterior aluminum ring with top and bottom cover plates, a copper block with inside cartridge heaters, and insulation material. To reduce oxidization of the heated surface and clogging in the orifices and pipes, distilled water was used. The plate used was taken out of the atomizer after each experiment and cleaned using an ultrasonic cleaner before the next test.

The arrangement of the copper block and the thermocouples is shown in Fig. 14.

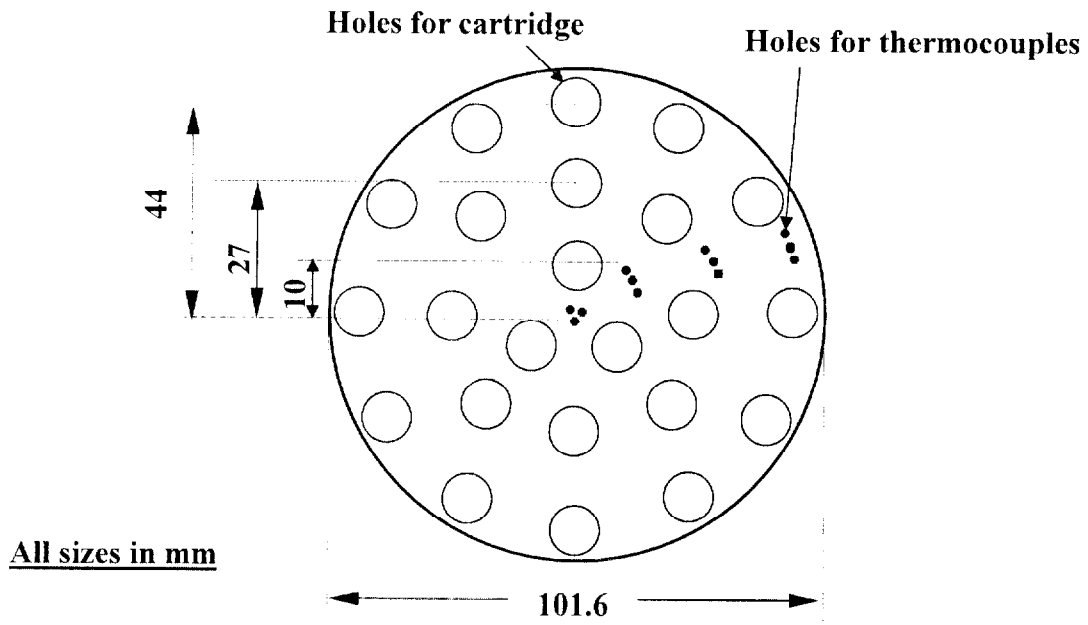

Figure 14. Temperature measurement locations on the heater.

The copper is oxygen-free, and the block 10 cm in diameter. The exposed surface is nickel-plated to a thickness of 50 μm. 23 cartridge heaters were obtained from OMEGA, each rated at 100 W maximum. Their positions were arranged in such a way that the block would be heated as uniformly as possible. Twelve K-type subminiature thermocouples were inserted into the copper block at 4 radial locations. There are 3 in each group, located at different depths to extrapolate the surface temperature. Holes for the cartridge heaters are 9.4 mm in diameter and a total of 23 are arranged in three concentric circles as shown in Fig. 14. The holes for the thermocouples are 1.6 mm in diameter and a total of 12 are located as shown in Fig. 14.

The copper block was surrounded by Cotronics Rescor 360 Ceramic Board insulation. This insulation was selected for its extremely low thermal conductivity (0.055 W/m·K at 260 °C and 0.108 W/m·K at 600 °C), its resistance to high temperature (continuous operating temperature limit is 1260 °C), its rigidity, and its machinability. There is a center hole in each insulation layer below the copper block to allow the thermocouples and cartridge heater leads to pass through.

A square, 1.59 mm thick Macor machineable ceramic cover was placed above the uppermost piece of the insulation layer, with a hole 10.16 cm in diameter in it for the exposed nickel-plated copper surface. The Macor sat on a ridge machined into the top aluminum cover plate. The exposed heater surface was maintained flush with the surrounding Macor plate by adjusting three screws beneath the insulation at the very bottom of the assembly. High temperature sealant 906 (Megnesia Adhesive from Cotronics) was used to fill the gap between the Macor and the aluminum cover plate.

Excess water flowed down along the exterior surface of the aluminum ring and was drained out through a hole in the slot, which was formed by the cylinder and the short ring mounted on the bottom plate.

Since the position of the Phase Doppler Particle Analyzer (PDPA) was fixed, the heater and the atomizer were moved together to measure droplets at different axial and radial locations. A three-dimensional motor controller was used to provide accurate relative positioning of the laser probe volume.

The twelve voltage signals from the thermocouples were received by the EXP-16 board (Computer Boards) and multiplexed into a single signal for amplification. A gain of 100 was used to achieve the largest voltage measurable and programmable by the CIO-DAS1402/12 board (from Computer Boards). The EXP-16 also contained a CJC (cold junction compensation) circuit for correcting thermocouple readings.

A schematic of the PDPA that was used to measure the sizes and velocities of the droplets is shown in Fig. 15. The PDPA consists of 5 major components: transmitter,

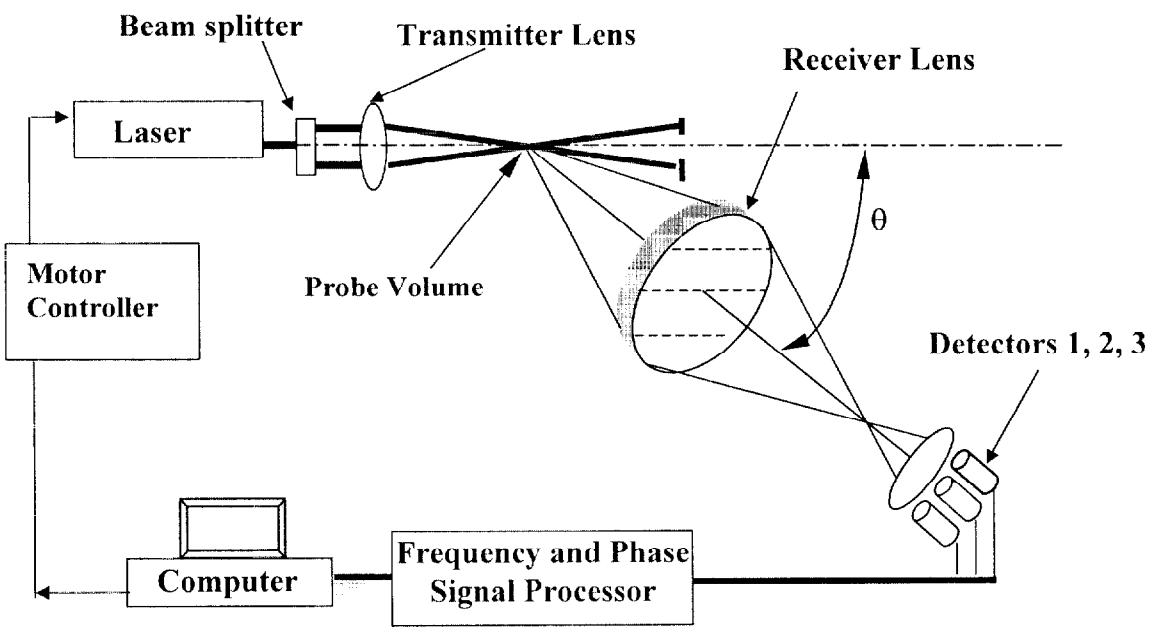

Figure 15. Schematic diagram of PDPA instrument

receiver, signal processor, motor controller box, and computer. The transmitter (Model 1100) contains a 10 mW, polarized Helium-Neon laser. The collimating lens was 300 mm, and the receiver lens was 1000 mm. Thus we could get the largest range for measuring droplet sizes. The forward scattering mode was used to obtain data.

For transparent particles, light scattered at 30 degrees to the forward direction is dominated by refraction. Droplets passing through the intersection of the two beams

scatter light which produces a far field interference fringe pattern. The spacing between these projected fringes is directly proportional to the drop diameter, but also depends on the light wavelength, beam intersection angle, drop refractive index (unless only reflected light is measured), and the location of the receiver. The PDPA obtains measurements of this fringe spacing via their image. As the fringes move past the detectors at the Doppler difference frequency, they produce identical signals but with a phase shift proportional to the fringe spacing. The temporal frequency of the measured signal is proportional to the particle velocity in the plane of the beams and orthogonal to the bisector of the beams. The spatial frequency of the interference fringe pattern is inversely proportional to the particle diameter.

Experiments were performed for different liquids, nozzle plates, flow rates and operating frequencies. The initial surface temperature of the copper was chosen to be 600 °C for water and 250 °C for Fluid 510. In addition, a base line data set with the heater at 25 °C was also obtained. For a given a nozzle plate and a given flow rate, the operating frequencies were changed to get different drop size and velocities. A frequency was chosen by visually observing the jet shape and ensuring that there were no satellite droplets breaking away from the main stream. A plastic curtain was used in the experiments to reduce the ambient disturbances. Measurements at different axial and radial locations within the spray were obtained by moving the heater and the nozzle assembly using a slide.

3.2 Numerical Methods

Droplets that arrive at the location of the fire have to pass through the hot environment. For designing suppression systems, models are routinely used to calculate droplet trajectories. These models have to account for buoyancy and evaporation. The data obtained using the PDPA can be used for assessing the accuracy of these models. During the course of the project, a model based on Lund and Sojka (1995) that accounts for coalescence and evaporation of droplets was evaluated using the data.

The influence of evaporation was evaluated through use of the d^2 law as described by Masters (1976):

$$\frac{dm}{dt} = 2\pi D_V \frac{p_V}{RT} ShD \tag{3}$$

where m is droplet mass, t is time, D_V is the mass diffusion coefficient, p_V is the vapor pressure, R is the ideal gas constant for the vapor, T is the temperature, Sh is the Sherwood number, and D is the drop diameter.

A change of variables converts the change in mass with respect to time in equation (3) to a change in diameter with respect to axial location. The resulting equation is:

$$\frac{dD}{dz} = \frac{4D_V p_V Sh}{\rho_l DRTV} \tag{4}$$

The remaining unknown variable, the Sherwood number, was calculated using the correlation found in Ranz and Marshall (1952):

$$Sh = 2 + 0.6\, Re^{0.5}\, Sc^{0.33} \tag{5}$$

where Re is the Reynolds number and Sc is the Schmidt number.

Calculations were made using equations (4) and (5), plus the definitions of Re and Sc, to determine the change in drop diameter with axial location for a particular size class. Since drop diameter was found to decrease by only 0.015 μm for every 1 cm of axial distance we conclude that the influence of evaporation is negligible for the hydrocarbon oil used in this investigation.

The extent to which droplet coalescence plays a role in increasing SMD was determined via a kinetic theory-based model. The model neglects viscous, gravitational and pressure forces. It is based on the coalescence of a droplet of size-velocity class i with a droplet of size-velocity class j to yield a droplet of size-velocity class k:

$$D_i + D_j \rightarrow D_k \tag{6}$$

From this relationship the rate equation for change in number of droplets of class i is:

$$\frac{dn_i}{dz} = \varepsilon\left(-\sum \frac{k_{ij}\eta_i\eta_j}{V_i} + \sum \frac{k_{ij}\eta_i\eta_j\alpha_{ij}}{V_i}\right)\forall_p \tag{7}$$

where η_i, the counts per unit volume for droplet class i, is defined as

$$\eta_i = \frac{n_i}{A_p t_{run} V_i} \tag{8}$$

k_{ij}, the collision frequency for droplets of class i colliding with those of class j, is defined as:

$$k_{ij} = \frac{\pi}{4}(D_i + D_j)^2 V_{ij} \tag{9}$$

and ε is the probability of a collision leading to coalescence. ε was determined by extrapolating the work of Jiang et al. (1992) to our fluids, and then approximating their impact parameter versus Weber number curves as straight lines. Such a procedure will over-estimate the probability of a collision leading to coalescence.

In equations (7) through (9), n_i represents the number of droplets in class i, A_p is the P/DPA probe area normal to the flow, t_{run} is the run time, V_i is the velocity of class i, $\forall_p$ is the P/DPA probe volume, and α_{ij} represents the diameter D_k that results from coalescence in equation (6).

Equations (7) through (9) were used to calculate the change in number of droplets for a particular class i with respect to axial location. Care must be taken when distributing the product mass and momentum over the appropriate size-velocity bins. The coarse-grained PDF technique of Sivathanu and Gore (1993) was therefore employed to keep computational evaluation of equation (7) tractable while ensuring spray mass and momentum conservation. Having calculated $\frac{dn_i}{dz}$ in this fashion, $\frac{dSMD}{dz}$ was determined by taking the derivative of SMD with respect to z.

$$\frac{dSMD}{dz} = -\frac{(\sum D_i^2 \frac{dn_i}{dz})(\sum n_i D_i^3)}{(\sum n_i D_i^2)^2} \tag{10}$$

Equation (10) was then used to calculate a change in the SMD due to coalescence of droplets with axial location. The results were compared with those obtained using the PDPA instrument.

3.3 Results and Discussion

The temperature field above the hot plate is shown in Fig. 16. The temperature is

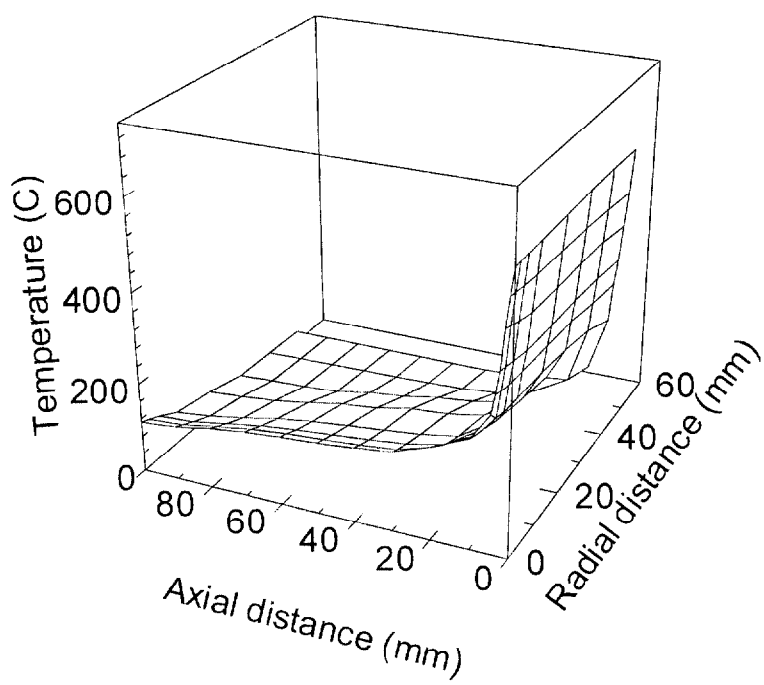

Figure 16. The temperature field at steady state above the hot plate.

600 ^{o}C just above the hot plate and rapidly decreases due to buoyancy induced entrainment. At an axial distance of 100 mm, the temperature is less than 200 ^{o}C at the

center line. The buoyancy induced velocity field is unsteady. However, the time-resolved velocity field was not measured in this experiment. The injector was located 250 mm above the hot plate in the centerline.

A steady k-ε-g model was used to try to predict the temperature field. The steady state k-ε-g model was modeled assuming a boundary layer flow. However, even under steady state conditions, the local velocity field had both positive and negative values. This could be readily visualized using smoke. The model does not have a mechanism to account for flow reversals. Therefore, the model predictions did not match the experimental observations. The model predictions are not provided in this report due to the very big divergence from the experimental observations. A 3-D large eddy simulation code was initiated to improve the model predictions. These calculations could not be completed within the reduced two year time frame of the project.

The change in droplet diameter with the distance from the injector is shown in Fig. 17. The PDPA results obtained using a cold plate and a hot plate are shown in the same

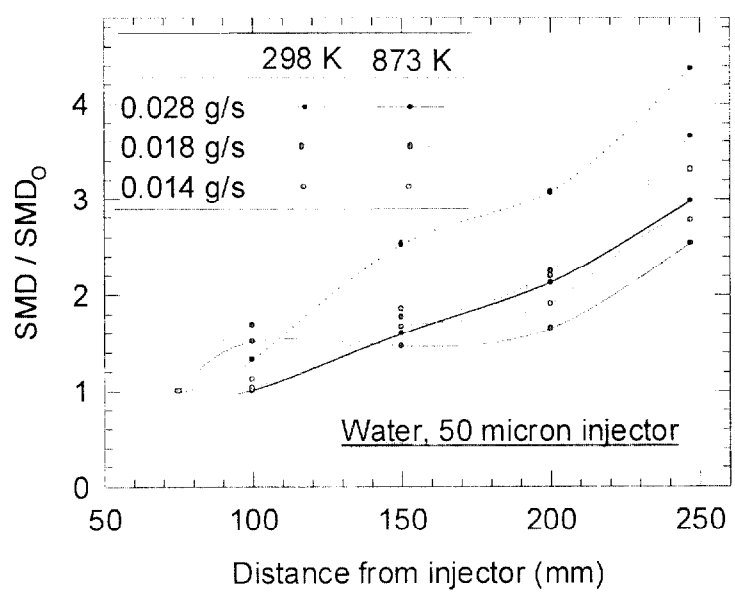

Figure 17. Change in SMD of the droplets with axial distance for water.

figure. The effects of coalescence are readily apparent. For both cases, the diameter of the droplets increase by approximately a factor of three by the time they arrive at the hot plate. For the hot surface, the droplet diameter increases only by a factor of two.

There could be two reasons for the lower drop diameters when the environment is hot. The first reason is that the buoyancy induced flow field affects local velocities significantly so as to lower coalescence. The second reason could be that evaporation of the droplets is reducing their SMD. These two effects can be separated using non-evaporating droplets.

Fluid 510 from Dow Corning was used to eliminate evaporation effects on the drop size history. When the fluid was sprayed onto the surface at 600 ^{o}C, a thick smoke was formed. This smoke prevented the PDPA from obtaining drop velocity and size data. In addition, the fluid formed a very hard coating on the copper plate. Therefore, the plate was cleaned, and the temperature reduced to 250 ^{o}C (below the flash point of Dow 510 Thermal Fluid).

The change in drop diameters with axial locations for Fluid 510 is shown in Fig. 18.

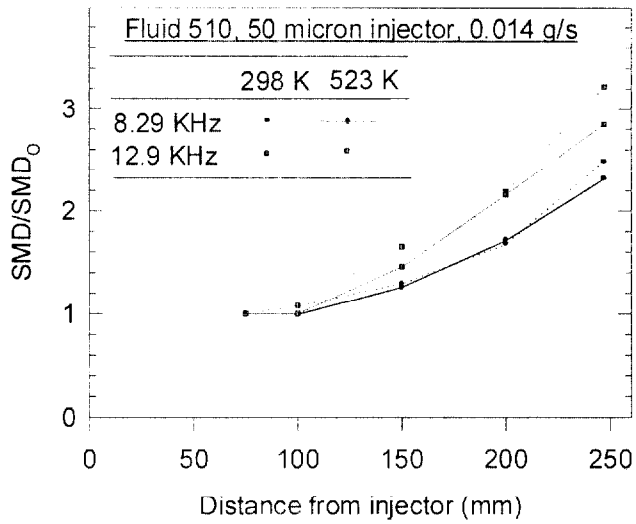

Figure 18. Change in SMD of the droplets with axial distance for Fluid 510.

Two different excitation frequencies, representing two different drop diameter distributions were used for the experiments. For both cases, it was found that the variation in SMD was identical irrespective of the temperature of the plate. Therefore, the buoyancy induced flow field does not significantly affect the coalescence of droplets. It is evaporation that is responsible for the lower SMD when the plate is hot.

To evaluate the coalescence model, the velocity and number density of the droplets is required. The velocity of the water droplets is shown in Fig. 19. It is clearly evident that the velocity of drops is affected significantly by buoyancy. The velocities are much lower when the plate is hot. This usually increases the droplet SMD since the lower velocities provide a longer time interval for coalescence.

The change in velocity with axial distance for three conditions using Fluid510 is shown in Fig. 20. Due to the lower temperatures attained, the change in velocity due to the buoyancy induced upward velocity of air is minimal. Similar results were obtained for the 20 micron nozzle.

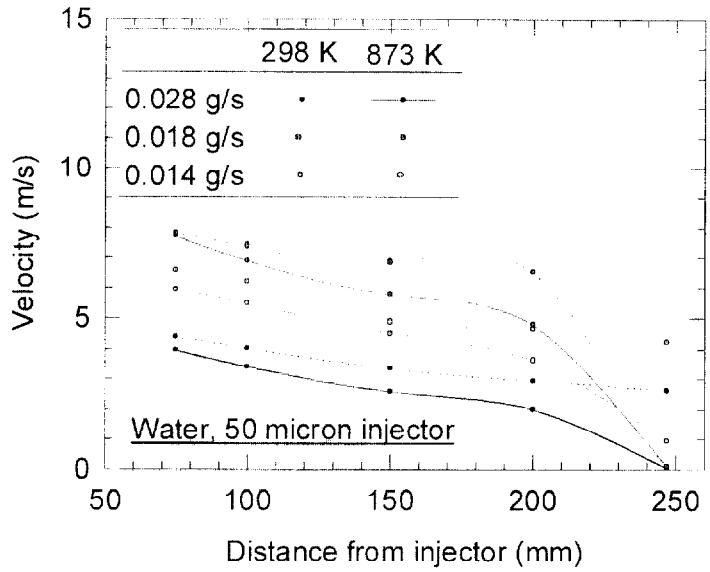

Figure 19. Variation in velocity with axial distance for water spray.

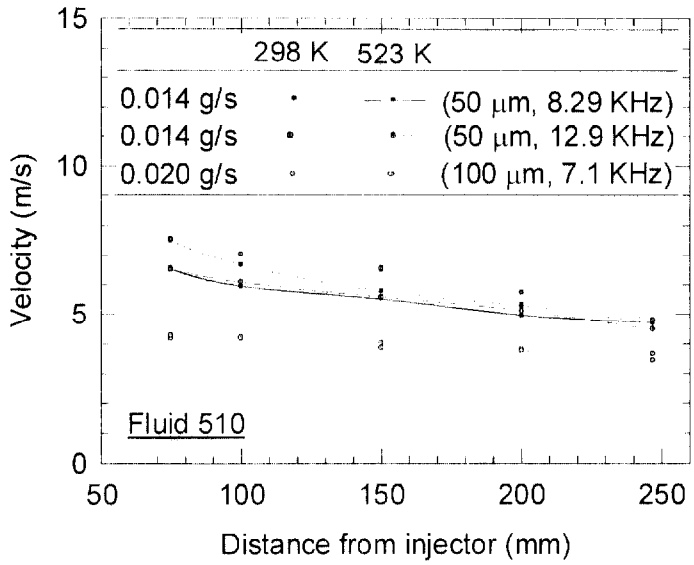

Figure 20. Variation in velocity with axial distance for Fluid 510.

In all cases, the drop diameter increases a factor of two or higher with downstream distance. Coalescence is the primary reason for the increase in drop diameter.

3.4 Preliminary Model Results

Preliminary results from modeling the change in SMD with diameter using Eq. 4 for coalescence and Eq. 10 for droplet evaporation differed significantly from the experimental data. The coalescence model predicts approximately two orders of magnitude lower changes in SMD with axial distance. The evaporation model suggests that the SMD of droplets change by less then 2% in all cases.

Improvements in the model using a Monte-Carlo based approach have to be pursued to delineate the effects of coalescence and evaporation. In addition, a more rigorous method of predicting the temperature field above the hot surface is needed to implement the Monte-Carlo simulations. In addition, wake effects are important in this study and they have to be incorporated into the models.

4. Summary and Conclusions

4.1 Important Findings

The flame spread rate in 'without backing' mode is found to be greater than in 'with backing' mode because flame spread in the former takes place on both sides. In the present study at ambient oxygen concentration, the heat transfer controlling fuel vapor evolution rate is the dominant factor controlling the flame spread rate.

The results of the experiments on flame spread in the presence of a water mist indicate the strong influence of surface loading in reducing flame spread rate. A correlation that can be used to obtain the optimal amount of water loading to extinguish fires was empirically developed. This correlation can be used to design systems that direct agents to the fire location to minimize the volume of suppressants required for extinguishment of fires.

The flame spread rate for the same liquid loading decreased slightly for smaller droplets. This effect was not very noticable for the range of drop sizes studied. Therefore, water loading, rather than the size of the droplets within the spray, is the more important parameter for flame extinguishment.

Droplet diameter and velocity measurements from a mono-disperse spray onto a hot plate showed that buoyancy had a significant impact on both droplet velocities and diameters. The velocity slows down to half the injection velocity, causing the faster and cooler droplets to collide and coalesce with the droplets in front of them near the surface of the hot plate. Therefore, in a real fire scenario, droplet coalesce is expected to be important. Coalescence of droplets was also found to be significant for non-evaporating fluids. Therefore, buoyancy induced drag on the droplet leads to a higher degree of coalescence in the spray.

For the temperatures obtained during the study, the change in drop diameters due to evaporation is much lower than that due to coalescence.

4.2 Significant Hardware Development

Three significant pieces of hardware were developed during the course of this project. The first is the wind tunnel that permits observation of flame spread under the influence of a water mist. The second is a well characterized hot surface for conducting drop-size and velocity histories for a spray impinging on a hot surface. The third is a Two Color Planar Pyrometer that allows the surface temperature to be obtained. The system was calibrated and an initial set of data obtained.

4.3 Recommendations for Future Research

Two coalescence and evaporation models evaluated during the first two years of the project were not successful in predicting drop size histories. Further evaluation of the droplet coalescence and evaporation model is required to delineate the effects of buoyancy and evaporation on drop size histories as the suppressant interacts with a fire. Reduction in the temperature of burning surfaces under a water mist have to be measured for more conditions to obtain a more accurate assessment of the optimal water loading required for fire extinguishments.

4.4 List of Publications

1. Fu, C., Sojka, P. E., and Sivathanu, Y. R., Water Mist Impingement onto a Heated Surface, Proceedings of the 5th Joint ASME/JSME Joint Thermal Engineering Conference, 1999.
2. Fu, C., Sojka, P. E., and Sivathanu, Y. R., On the Interaction Between Evaporating Sprays and Heated Surfaces, Proceedings of the 12th Annual Conference on Liquid Atomization and Spray Systems, 1999.
3. Sivathanu, Y., Oke, H. P., Fu, C., and Sojka, P.E., Droplet Interaction with Hot Surfaces, NGP Annual Report, 1998.
4. Oke, H. P., Sojka, P. E., and Sivathanu, Y. R., Flame Spread over Polymethylmethacrylate with Opposed Air Flow, submitted to the Journal of Fire Safety.
5. Harsh P. Oke, "An Experimental Study of Flame Spread over PMMA Subject to a Water Mist" M.S. Thesis, School of Mechanical Engineering, Purdue University, November, 1999.
6. Chunming Fu, "Droplet Interactions with a Hot Surface," M.S. Thesis submitted to the School of Mechanical Engineering, Purdue University, March, 2000.

5. Implications for Further Research

The correlation obtained during the study shows that the reduction in flame spread rate can be modeled empirically as a function of the local mass loading. The influence of droplet diameter is minimal. The implication is that a well designed and directed spray nozzle can be used to extinguish the fire with water as effectively as a flooding nozzle working with a more efficient suppressant, since the optimal local liquid loading required can be calculated a priori. In addition, secondary collisions and coalescence can cause small mist sprays to reach the fire as large drops

References

Apte, V.B., Bilger, R.W., Green, A.R. and Quintere, J.G., 1991, *Combust.Flame*, vol. 85, p. 169.

Braidech, M.M., Neale, J.A., Matson, A.F., and Dufour, R.E., 1955, "*The Mechanism of Extinguishment of Fire by Finely Divided Water*," *Underwriters Laboratories Inc. for the National Board of Fire Underwriters*, N.Y., p. 7.

Brenn, G., HelpiÖ, T. and Durst, F., 1997, *Chemical Engineering Science*, vol. 52, p. 237.

Coppalle, A., Nedelka, D., and Bauer, B., 1993, *Fire Safety Journal*, 20, p. 241.

De Ris, J., 1969, *Twelfth Symposium (International) on Combustion*, The Combustion Institute, Pittsburgh, p. 241.

DiMarzo, M., Kavoosi, and Klassen, M. (1989), "*Transient Cooling of a Hot Surface by Droplets Evaporation*," Report prepared for the National Institute of Standards and Technology, NIST-GCR-89-559, University of Maryland, College Park, MD.

DiMarzo, M., and Evans, D. D. (1986), "*Evaporation of Water Droplet Deposited on a Hot High Thermal Conductivity Solid Surface*," National Bureau of Standards Interagency/Internal Report, NBSIR 86-3384.

Dingel, B. E., 1997, "*An Experimental and Theoretical Study of Air/Water Mist Impingement Cooling*", M.S. thesis, Mechanical Engineering, Purdue University.

Fernandez-Pello, A. C., Ray, S. R., and Glassman, I., 1978, *Combust. Sci. Tech.*, vol. 19, p. 19.

Fernandez-Pello, A. C., Ray, S. R., and Glassman, I., 1981, *Eighteenth Symposium (International) on Combustion*, The Combustion Institute, Pittsburgh, pp. 579.

Fox, R.W., and McDonald, A.T., 1995, *Introduction to Fluid Mechanics*, John Wiley & Sons (SEA) Pte. Ltd., Singapore.

Haji-Sheik (1988), *Handbook of Numerical Heat Transfer*, John Wiley & Sons Inc., NY.

Hicks, P. G., and Senser, D. W., 1995, *J. of Fluids Engg.*, vol. 117, p. 713.

Howell, J. R. (1968), *Advances in Heat Transfer*, vol. 5, Academic Press, New York, p. 1.

Jiang, Y. J., Umemura, A., and Law, C. K., 1992, *J. Fluid Mech.*, vol. 234, pp. 171.

Kahn, H., and Marshall, A. W., 1953, *J. Operations Res. Society of America*, vol. 1 p., 263.

Kline, S.J., and McClintock, F.A., 1953, *Mechanical Engineering*, 75(1), p. 3.

Kwok, K. C., 1991, *A Fundamental Study of Air-Spray Painting*, Ph. D. Thesis, Mechanical Engineering Department, University of Minnesota.

Lanore, J. M., 1971, Nucl. Sci. Eng., vol. 45, pp. 66-72.

Lastrina F.A., Magee R.S., and McAlevy III, R.F., 1971, *Thirteenth Symposium (International) on Combustion*, The Combustion Institute, Pittsburgh, p. 935.

Loh, H.-T. and Fernandez-Pello, A.C., 1984, *Twentieth Symposium (International) on Combustion*, The Combustion Institute, Pittsburgh, p. 1575.

Lugar, J. R., 1979, "*Preliminary Test Results of Fine Water Mist Fire Protection Systems Study*," David W. Taylor Navel Ship R&D Center, Maryland, 1980.

Masters, K., *Spray Drying*, 2nd Edition, John Wiley and Sons, New York, 1976.

Mawhinney, J. R., Dlugogorski, B. Z., and Kim, A. K., 1994, *Proceedings of the Fourth International*

Symposium on Fire Safety Science, Ottawa, CA, p. 47.

Perzak, F.J. and Lazzara, C.P., 1992, *Twenty-Fourth Symposium (International) on Combustion*, The Combustion Institute, Pittsburgh, p. 1661.

Rasbash, D.J., Rogowski, Z.W., and Stark G.W.V., 1960, *Combust. Flame*, 4, pp. 223.

Ranz, W. E., and Marshall, W. R, 1952, *Chemical Engineering Progress*, vol. 48, p. 141.

Sivathanu, Y. R., and Gore, J. P., 1993, *JQSRT*, vol. 49, p. 269.